# Decay properties of $^{68,69,70}$Mn: Probing collectivity up to A=44 in Fe isotopic chain

G. Benzoni[a,*], A.I. Morales[a,b], H. Watanabe[c,d], S. Nishimura[c], L. Coraggio[e], N. Itaco[e,f], A. Gargano[e], F. Browne[g,c], R. Daido[h], P. Doornenbal[c], Y. Fang[h], G. Lorusso[c], Z. Patel[i,c], S. Rice[i,c], L. Sinclair[j,c], P.-A. Söderström[c], T. Sumikama[k], J. Wu[c], Z.Y. Xu[l,c], R. Yokoyama[m], H. Baba[c], R. Avigo[a,b], F.L. Bello Garrote[n], N. Blasi[a], A. Bracco[a,b], F. Camera[a,b], S. Ceruti[a,b], F.C.L. Crespi[a,b], G. de Angelis[o], M.-C. Delattre[p], Zs. Dombradi[q], A. Gottardo[o], T. Isobe[c], I. Kuti[q], K. Matsui[l], B. Melon[r], D. Mengoni[s,t], T. Miyazaki[l], V. Modamio-Hoybjor[o], S. Momiyama[l], D.R. Napoli[o], M. Niikura[l], R. Orlandi[u,v], H. Sakurai[c,l], E. Sahin[n], D. Sohler[q], R. Taniuchi[l], J. Taprogge[w,x], Zs. Vajta[q], J.J. Valiente-Dobòn[o], O. Wieland[a], M. Yalcinkaya[y]

[a] *Istituto Nazionale di Fisica Nucleare, Sezione di Milano, Via Celoria 16, 20133 Milano, Italy*
[b] *Dipartimento di Fisica dell'Università degli Studi di Milano, Via Celoria 16, 20133 Milano, Italy*
[c] *RIKEN Nishina Center, 2-1 Hirosawa, Wako, Saitama 351-0198, Japan*
[d] *IRCNPC, School of Physics and Nuclear Energy Engineering, Beihang University, Beijing 100191, China*
[e] *Istituto Nazionale di Fisica Nucleare, Sezione di Napoli, Napoli, Italy*
[f] *Dipartimento di Fisica dell'Università di Napoli Federico II, Napoli, Italy*
[g] *School of Computing, Engineering and Mathematics, University of Brighton, Brighton, United Kingdom*
[h] *Osaka University, Osaka, Japan*
[i] *Department of Physics, University of Surrey, Guildford, United Kingdom*
[j] *University of York, York, United Kingdom*
[k] *Tohoku University, Sendai, Japan*
[l] *Department of Physics, University of Tokyo, Hongo 7-3-1, Bunkyo-ku, 113-0033 Tokyo, Japan*
[m] *CNS, University of Tokyo, Tokyo, Japan*
[n] *University of Oslo, Olso, Norway*
[o] *Istituto Nazionale di Fisica Nucleare, Laboratori Nazionali di Legnaro, Legnaro, Italy*
[p] *IPNO Orsay, Orsay, France*
[q] *MTA Atomki, Debrecen, Hungary*
[r] *INFN sezione di Firenze, Firenze, Italy*
[s] *Dipartimento di Fisica dell'Università degli Studi di Padova, Padova, Italy*
[t] *Istituto Nazionale di Fisica Nucleare, Sezione di Padova, Padova, Italy*
[u] *Instituut voor Kern- en StralingsFysica, K.U. Leuven, Belgium*
[v] *Advanced Science Research Center, JAEA, Tokai, Ibaraki, Japan*
[w] *Instituto de Estructura de la Materia, CSIC, E-28006 Madrid, Spain*
[x] *Departamento de Fisica Teórica, Universidad Autónoma de Madrid, E-28049 Madrid, Spain*
[y] *Department of Physics, Istanbul University, Istanbul, Turkey*

**Abstract**

The $\beta$ decays $^{68}$Mn $\rightarrow$ $^{68}$Fe, $^{69}$Mn $\rightarrow$ $^{69}$Fe and $^{70}$Mn $\rightarrow$ $^{70}$Fe have been measured at the RIBF facility at RIKEN using the EURICA $\gamma$ spectrometer combined with an active stopper consisting of a stack of Si detectors. The nuclei were produced as fission fragments from a beam of $^{238}$U at a bombarding energy of 345 MeV/nucleon impinging on a Be target and selected using the BigRIPS separator. Half-lives and $\beta$-delayed neutron emission probabilities have been extracted for these decays, together with first experimental information on excited states populated in $^{69,70}$Fe. The data indicate a continuously increasing deformation for Fe isotopes up to A=70. This is interpreted, as for Cr isotopes, in terms of the interplay between the quadrupole correlations of the $\nu 1d_{5/2}$ and $\nu 0g_{9/2}$ orbitals and the monopole component of the $\pi 0f_{7/2}$ - $\nu 0f_{5/2}$ interaction.

*Keywords:*
*PACS:* 23.40.-s,27.50.+e

Magic numbers, originating from large energy gaps in the shell structure of the single-particle states, constitute one of the fundamental features governing nuclear structure. The access to new exotic species, where the number of protons (Z) and neutrons (N) is highly asymmetric, showed the onset of new magic numbers and an evolution of shell gaps driven by the enhanced role of pairing interactions and of tensor terms [1, 2]. These interesting findings, obtained using radioactive beams and confirmed by the many developments in shell model calculations, are based on a very extensive experimental and theoretical work. Presently they are motivating additional experimental and theoretical investigations addressing these important issues on shell structure in nuclei further away from stability. Indeed, the evolution of shell structure depends strongly on the occupations of proton and neutron orbitals near the Fermi surface and on their mutual interactions, and, therefore, it can only be identified via systematic studies of nuclear properties in different isotopic and isotonic chains.

In this context, one region in the chart of nuclides attracting particular attention is that around $^{78}$Ni, a key region to study the path toward the N=50 shell closure and its implications on the astrophysical r-process [3, 4, 5] for nucleosynthesis. In particular, the study of the evolution of excited states for the Cr, Fe, Zn, Ge isotopes provides a stringent test to shell model calculations leading to N=50.

The existence of the sub-shell closure at N=40 was proposed since a relatively large gap separates the pf shell from the neutron $g_{9/2}$ single-particle state. This picture was initially confirmed by the measurement of a large energy of the first $2^+$ state in $^{68}$Ni and, more recently, of its B(E2) value: the level energy is much higher than the neighbouring even-even isotopes [6], while the B(E2) is indeed the smallest in the Nickel chain [7]. Langanke and collaborators [8] argued, however, by comparing several approaches, that the small experimental B(E2) value could not be a conclusive argument in favour of a shell closure, since the missing strength lies in excited states above 4 MeV. Recent mass measurements support this picture, implying a relatively small shell gap [9].

The study of nuclei around $^{68}$Ni, in particular removing protons from the $0f_{7/2}$ orbital, confirmed the picture of the vanishing of the shell closure at N=40: the observed rapid drop in the energies of the $2^+$ states in Fe (Z=26) [10, 11, 12, 13, 14] and Cr (Z=24) [15, 16] isotopic chains points to an increased collectivity in these nuclei, which is expected to reach its maximum at N=40 and N=38 in Fe and Cr, respectively [17]. It has also been suggested that the ground states of $^{62-68}$Fe are dominated by spherical configurations, at variance with the ground states of $^{60-64}$Cr, which are associated to deformed shapes [18].

A very recent intermediate Coulomb excitation experiment [19] extended the measurement of the B(E2:$0^+_1 \rightarrow 2^+_1$) which were known only up to $^{66}$Fe [13, 14] and gave the first result at N=40 in the Cr chain. The large B(E2) value found for $^{68}$Fe suggests an increased collectivity in this nucleus as compared to the lighter isotopes.

This large body of experimental works suggest that shell-model calculations have to include the neutron $1d_{5/2}$ orbital in order to reproduce the large quadrupole collectivity found in these isotopic chains. These computational-heavy calculations predict an onset of deformation for N=40 in the Fe chain and at N=38 in the Cr one. Chromium isotopes are expected to show maximum deformations in this region, being the proton $0f_{7/2}$ orbital half filled [17, 20, 21].

The work presented in this letter is intended to extend the experimental knowledge of the isotopic chain of Fe in the neutron rich side by new measurements that have provided the half-lives and $\beta$-delayed neutron emission probabilities of their $\beta$-decaying parents $^{68,69,70}$Mn, and the excitation energies of the first excited states up to N=44. These data are compared with the experimental systematics for Ni, Fe, Zn, Ge, and with recent shell model calculations to deduce the orbitals involved in these new excitations and collective effects, supporting the picture of an increasing deformation while adding neutrons.

The experiment here discussed was performed at RIKEN as part of the EURICA campaign at the Radioactive-Isotope Beam Factory (RIBF) facility. The nuclear species were produced by means of in-flight fission of a $^{238}$U beam at a bombarding energy of 345 MeV/nucleon. The experiment collected data for an equivalent time of 3 days with an average primary beam intensity of 10 pnA.

The resulting fragments were separated in the BigRIPS separator, by the use of degraders at the intermediate dispersive foci [27]. The cocktail beam was transported through the ZeroDegree spectrometer down to the final focal plane where it was then slowed down in an Al degrader to ensure the implantation of the species of interest in the 5 silicon detectors of the WAS3ABi array [28]. The total count rate at the final focal plane was limited to 100 pps to ensure correct ion-$\beta$ correlations.

*corresponding author
*Email address:* giovanna.benzoni@mi.infn.it
(G. Benzoni)

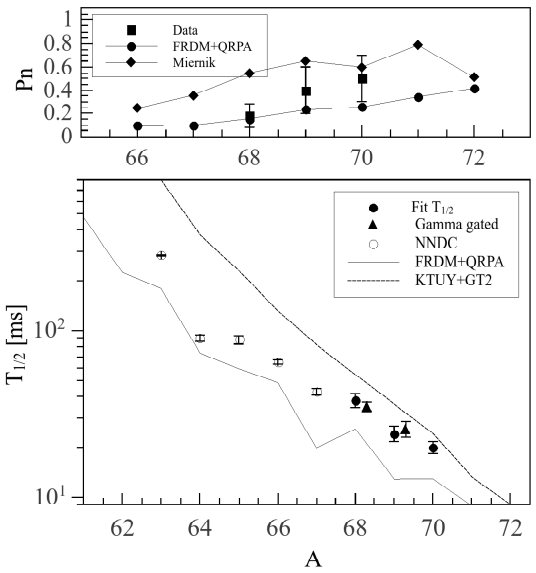


Figure 1: Bottom panel: systematics of half-lives in the Mn chain: open symbols are values found in the literature [22], while the filled ones are obtained from the analysis described here. Circles are the results of a multi-parameter fit extending to the grand-daughter decay products, and including the delayed-neutron emission branches, while triangles are obtained with gates on $\gamma$ transitions specific of the daughter nucleus. An offset has been introduced in the two sets of data for a better comparison of the results. The experimental values are compared to two different calculations: FRDM+QRPA [23] (solid line) and KTUY+GT2 [24, 25] (dashed line). In the top panel, the $\beta$-delayed neutron emission probabilities are shown. The filled squares are the values extracted from our analysis, while filled dots are values tabulated in Ref. [23] and filled diamonds are from Ref. [26].

The Si array was surrounded by the EURICA spectrometer consisting of 12 EUROBALL HPGe cluster detectors [29]. Eighteen small volume $LaBr_3$(Ce) scintillator detectors were also employed for fast-timing measurements [30]. The yields for the mother nuclei, after implantation, were: 6700 $^{68}$Mn ions, 4300 $^{69}$Mn ions and 400 $^{70}$Mn ions.

Once the different isotopes were identified, they were associated to their subsequent $\beta$ decay by imposing spatial and temporal correlations: we requested the $\beta$ event to be registered in the pixel where the implantation occurred, or in the closest neighbours, and, in addition, a time correlation window was imposed. All $\beta$ events satisfying these conditions were associated with an implant. Typical $\beta$ efficiency for $^{68,69,70}$Mn was estimated to be around 60%.

Since the half-lives of the Mn isotopes of interest are similar to those of their Fe and Co successors [22], a fit to the Bateman equations [31], including the activity of daughter and grand-daughter nuclei, was performed for each species. Half-lives of decay successors were fixed to their literature values [22] if known. The $\beta$-delayed neutron emission branch is expected to contribute significantly to the total decay rate of the neutron-rich Mn isotopes [23]. Since $\beta$-delayed neutron emission probabilities ($P_n$) are not measured in $^{68-70}$Mn, they have been deduced as free parameters in the fit. When the statistics were sufficiently high, the half-lives were cross-checked with values obtained gating on de-exciting $\gamma$-ray transitions of the daughter nuclei, by fitting the decay spectrum with an exponential decay curve.

The evaluated half-lives for the discussed decays are the following: $^{68}$Mn $\rightarrow$ $^{68}$Fe $T_{1/2}$= 38.3 $\pm$ 3.6 ms, and $T_{1/2}$= 35.2 $\pm$ 2 ms gating on $\gamma$ transitions (521+865+1250+1514 keV); $^{69}$Mn $\rightarrow$ $^{69}$Fe $T_{1/2}$= 24.1 $\pm$ 2.6 ms, and $T_{1/2}$= 25.8 $\pm$ 2.8 ms with gates on the following $\gamma$ rays: 135, 325, 355, 521, 1207 keV. In the case of $^{70}$Mn $\rightarrow$ $^{70}$Fe the half-life could only be extracted from a fit of the decay curve, resulting in $T_{1/2}$= 19.9 $\pm$ 1.7 ms. Error bars include both statistical and systematic errors, calculated from the $\chi$-square minimization described earlier.

The measured half-lives are reported in the bottom panel of Fig. 1: filled circles represent the values extracted from a fit to the $\beta$-decay spectrum, while filled triangles are obtained gating on de-exciting $\gamma$ transitions in the daughter nuclei.

The values extracted from this analysis are shown together with the half-lives found in literature for lighter Mn isotopes (open dots) [22].

A comparison to theorical predictions is given in the figure: the solid line shows predictions from the FRDM+QRPA model [23], while the dashed line from the KTUY+GT2 model [25, 24]. The first theoretical approach is based on the FRDM mass model and calculates the Gamow-Teller (GT) transition strength with a quasiparticle random-phase approximation approach (QRPA). In this framework first-forbidden (FF) transitions are evaluated on the basis of statistical gross theory. The KTUY+GT2 theoretical model is instead based on the KTUY mass formula combined with the second generation of gross theory for GT and FF transitions. If the first model has been extensively used to

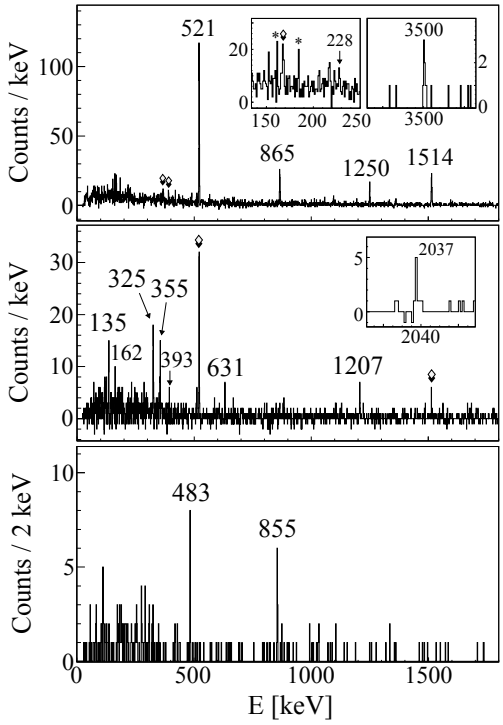


Figure 2: $\beta$-delayed $\gamma$-decay spectra following the decays $^{68}$Mn $\rightarrow$ $^{68}$Fe (upper panel), $^{69}$Mn $\rightarrow$ $^{69}$Fe (middle panel) and $^{70}$Mn $\rightarrow$ $^{70}$Fe (bottom panel). Transitions belonging to $^{68,69,70}$Fe are labelled, while transitions populating the $\beta$-n channel are indicated by diamonds. The asterisks indicate transitions depopulating states in the grand-daughter nucleus.

predict half-lives of nuclei in or close to the r-process path, the more recent one, KTUY+GT2, has been recently proven to have a good predictive power in nuclei around $^{78}$Ni and in the A$\approx$130 mass region [32, 33].

Experimental data points lie in between the two theoretical models: while the FRDM+QRPA model seems to show a similar trend, it systematically underestimates the values by a factor of 1.5-2; on the other hand, the predictions given by the KTUY+GT2 approach show a much steeper behaviour than seen experimentally, and get closer to the experimental values for the most exotic isotopes. FRDM+QRPA calculations predict an increased half-life at N=68, which could hint to a more stable configuration of this nucleus, together with an enhanced staggering in the odd-mass isotopes. This behaviour is not present in the experimental data, which show a smoother trend.

In the top panel of Fig. 1 we report the $P_n$ values extracted, for the first time, from the fit described earlier on. Previous half-life measurements either used theoretical values [10], or did not include explicitly this decay branch in the determination of the half-lives [12]. The $\beta$-delayed neutron-emission branch starts to have a sizable value already for mass A=68, and we see a steep increase for masses 69 and 70. Predictions by FRDM+QRPA (filled dots) start deviating from the experimental values at mass 69, pointing to a non-correct evaluation of the decay strength above the neutron separation energy for these exotic nuclei.

On the other hand, very recent predictions based on a phenomenological effective density model [26, 34, 35], which well account for $P_n$ values in various regions of the decay chart, overestimate the beta-delayed emission probability at low neutron numbers, thus implying an early deviation of the $\beta$-decay path. This model seems instead to better account for heavier isotopes, even if it shows an unusual staggering behaviour, with $P_n$ values decreasing for the odd-N isotopes. The present results indicate that more refined approaches, describing in detail the microscopic structure above the neutron separation energy, are required for a better reproduction of $P_n$ values.

Though total beta-delayed neutron-emission probabilities are of foremost importance for r-process nucleosynthesis calculations and reactor operation, at present there are $\sim$150 $P_n$ values experimentally determined [36]. The need of $P_n$ inputs for these applications has led to the development of models that calculate them from systematics, usually in nuclei near stability. The measurement of $P_n$ values in more exotic nuclei is hence particularly helpful to test their applicability towards the neutron drip line.

Figure 2 shows the energy spectra following the decays $^{68}$Mn $\rightarrow$ $^{68}$Fe (top panel), $^{69}$Mn $\rightarrow$ $^{69}$Fe (middle panel), and $^{70}$Mn $\rightarrow$ $^{70}$Fe (bottom panel). All spectra are obtained requiring an ion-$\beta$ correlation time window spanning 5 half-lives. Transitions belonging to each decay are labelled, while diamonds and asterisks mark transitions in the $\beta$-n channel and daughter decay, respectively.

We confirm the $\beta$-decay spectrum of $^{68}$Mn reported previously in Refs. [12, 37], even if we see a different relative population of the transitions at 1250 keV and 1514 keV, with the latter being more intense than the first, while Liddick et al. [12] reported similar intensity for those lines. The statistics for this decay allow to perform $\gamma - \gamma$ coincidence studies, which support the level ordering shown in Fig. 3. Relative intensities and coincidence $\gamma$ transitions are reported in columns 2 and 3 of Tab. 1.

Decay transitions are reported for the first time for

Table 1: $\gamma$-ray energies and relative intensities for the decay $^{68}$Mn $\rightarrow$ $^{68}$Fe (columns 1 and 2) and $^{69}$Mn $\rightarrow$ $^{69}$Fe (columns 4 and 5). Column 3 reports transitions found in coincidence in the decay of $^{68}$Fe.

| $^{68}$Mn $\rightarrow$ $^{68}$Fe | | | $^{69}$Mn $\rightarrow$ $^{69}$Fe | |
|---|---|---|---|---|
| $E_\gamma$ [keV] | $I_{rel}$ [%] | Coincidences | $E_\gamma$ [keV] | $I_{rel}$ [%] |
| 228.5* | 3(2) | 521, 1514 | 135.0 | 58 (15) |
| 521 | 100(10) | 865, 1250, | 162.4 | 16 (12) |
| | | 1514 | 325.1 | 100 (24) |
| 865 | 38(7) | 521 | 355.3 | 28 (18) |
| 1250 | 16(6) | 228.5, 521 | 393.3 | 22 (4) |
| 1514 | 46(8) | 521, 1250 | 521** | |
| 3500* | 11(3) | | 631.5 | 7 (4) |
| | | | 1207.8 | 54 (11) |
| | | | 1514** | |
| | | | 2037 | 44(13) |

*transitions not placed in the level scheme in Fig. 3; **$\beta$-n channel

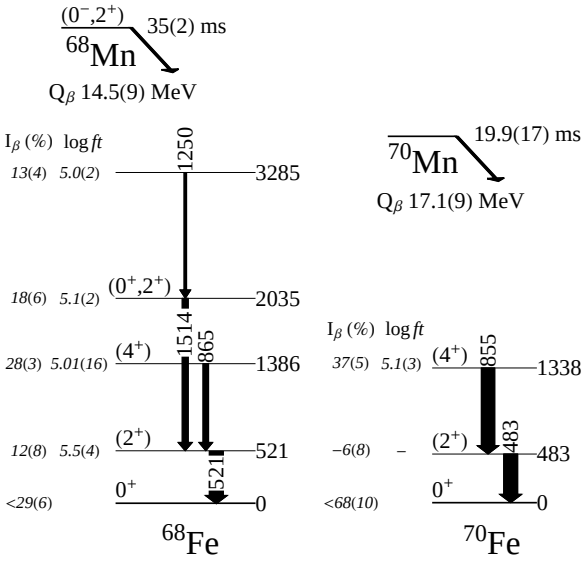


Figure 3: Partial level schemes following the $\beta$ decays $^{68}$Mn $\rightarrow$ $^{68}$Fe (left) and $^{70}$Mn $\rightarrow$ $^{70}$Fe (right). $Q_\beta$ values are taken from ref. [40].

$^{69}$Mn $\rightarrow$ $^{69}$Fe. In addition to the limited statistics collected for this channel, the decay of $^{69}$Mn is expected to be fragmented over a number of states, thus preventing the observation of $\gamma - \gamma$ coincidences. Table 1 reports the energy and relative intensity of the $\gamma$ transitions populated in $^{69}$Mn $\rightarrow$ $^{69}$Fe (columns 4 and 5). The intensities have been normalized to that of the 325-keV line, which, by analogy to the spectra of the neighbouring odd-mass isotopes [38, 39], is expected to feed the ground state.

The strong population of the 521-keV and 1514-keV transitions seen in the decay spectrum of $^{69}$Mn points to a large neutron-emission branch, in line with the value of 40(20)% extracted by the fit discussed previously. Following the $\beta$ and $\beta$-n decay to the grand-daughter, in order to account for ground-state feeding, we obtain a $P_n$ value of 50(20)%, for the full chain $^{69}$Mn$\rightarrow$$^{69}$Fe $\rightarrow$$^{69}$Co.

It is to note that the delayed-neutron branch seems to be mainly decaying to the states at 521 keV and at 2035 keV in $^{68}$Fe, and not to the state at 1386 keV: the 865-keV line, which is strongly populated in the direct decay, is not seen in the $\beta$-n branch of $^{69}$Mn. This might indicate a preferential population of specific states in the $\beta$-delayed neutron emission process.

In the bottom panel of Fig. 2, we show, for the first time, $\gamma$-ray transitions following the decay $^{70}$Mn $\rightarrow$ $^{70}$Fe. $^{70}$Mn is a hard-to-reach nucleus, and it has to be stressed that this spectrum follows the implantation of 400 ions only, proving the efficiency and selectivity achievable with the EURICA setup. From systematics we associate the 483-keV line to the $2^+ \rightarrow 0^+$ transition and the 855-keV line to the $4^+ \rightarrow 2^+$ transition.

The proposed level schemes following the $\beta$ decay of even-mass isotopes are shown in Fig. 3. At variance with the previous study [12], which reported a value <6%, the state at 2035 keV has an apparent $\beta$ feeding of 18(6)%, and we also attribute a lower feeding to the ground state, <29(6)%. The comparison of the decay patterns of $^{68}$Mn $\rightarrow$ $^{68}$Fe and $^{70}$Mn $\rightarrow$ $^{70}$Fe shows a sudden change: in the case of $^{70}$Mn $\rightarrow$ $^{70}$Fe the feeding seems to preferably go to the proposed $4^+$ state, while the $2^+$ state is mainly fed by internal decay coming from higher-lying states. The sudden change of the spin population in the daughter nuclei indicates different spin of the ground state of the mother nuclei.

The experimental results have been compared to a shell-model calculation performed with the CD-Bonn NN potential in the $V_{low-k}$ approach, described thouroghly in Refs. [41, 42], including, in the model space, the proton $0f_{7/2}$ and $1p_{3/2}$ orbitals and the neutron $1p_{3/2}$, $1p_{1/2}$, $0f_{5/2}$, $0g_{9/2}$ and $1d_{5/2}$ orbitals. The recent calculations reported in Ref. [21] have been extended, in the current work, to the $^{68,70}$Fe isotopes.

The shell-model calculation gives, for $^{68}$Fe, the $2^+_1$ state at 545 keV and a $4^+_1$ state at 1434 keV, in good agreement with the experimental values of 521 and 1386 keV. The state at 1386 keV has been proposed as the yrare $2^+_2$ state in Ref. [12]. This assignment has been made according to shell-model calculations excluding the $1d_{5/2}$ orbital from the neutron model space. In order to confirm that the removal of this orbital leads

to an inversion of the $4_1^+$ and $2_2^+$ states, we have performed shell-model calculations in a reduced neutron-model space consisting of only four orbitals: our calculations provide the $2_2^+$ level as second excited state, and the energy of the $4^+$ state increases to 1777 keV, which is in agreement with the value of 1752 keV proposed in Ref. [12].

We propose the level ordering and tentative spin-parity assignments shown in the left part of Fig. 3: the first excited state, at 521 keV, is proposed to be the first $2^+$ state, and the level at 1386 keV is tentatively assigned as $J^\pi=4^+$. The state at 2035 keV is interpreted as a low-J state, showing a branching ratio similar to that of the $2^+$ state: this can be either the second $2^+$ state or a second $0^+$ state. No direct ground-state decay from this state is observed.

Our shell model calculations predict, in the mother nucleus $^{68}$Mn, a large number of states within few tens of keV, the ground state having $J^\pi=0^-$ and the first excited state, at 19 keV, $J^\pi=2^+$ . The observed decay pattern, mainly feeding low-J states, points to a J<3 assignment for the ground state of $^{68}$Mn, consistent with shell-model calculations. The present data are, most likely, affected by the pandemonium effect [43], and therefore, the assignment proposed is tentative.

In the case of $^{70}$Fe, we propose the level scheme shown on the right of Fig. 3: the first excited state, at 483 keV, is interpreted as the first $2^+$ state, while the second, at 1338 keV is interpreted as the first $4^+$ state, in analogy with the systematics of the previous even-even isotope. This tentative assignment is additionally reinforced by our shell-model calculations, performed in the larger model space, which predict the first $2^+$ state at an energy of 487 keV and the first $4^+$ state at 1359 keV.

In figure 4 we report the energies of the first excited states measured in the isotopic chains right below (Cr and Fe) and above (Zn and Ge) the Z=28 closed-shell Ni chain. The evolution of the $2^+$ energies is shown in the top panel, while that of the $4^+$ energies in the middle panel. Level energies known prior to this study are taken from Ref. [22].

The comparison of the different isotopic chains show that the Fe chain has the typical signature for an increasing deformation, and this trend is confirmed by the energies of the $2^+$ and $4^+$ states in $^{70}$Fe reported in this letter for the first time.

This tendency is also clearly seen in the $R_{4/2}$ ratio between the excitation energies of the $4^+$ versus the $2^+$ states: the increasing behaviour of the $R_{4/2}$ for N=42,44 is confirmed and points to a continuous increase in collectivity, owing to the interaction of the neutron $1d_{5/2}$ with the proton $0f_{7/2}$ orbitals. Moreover the developed

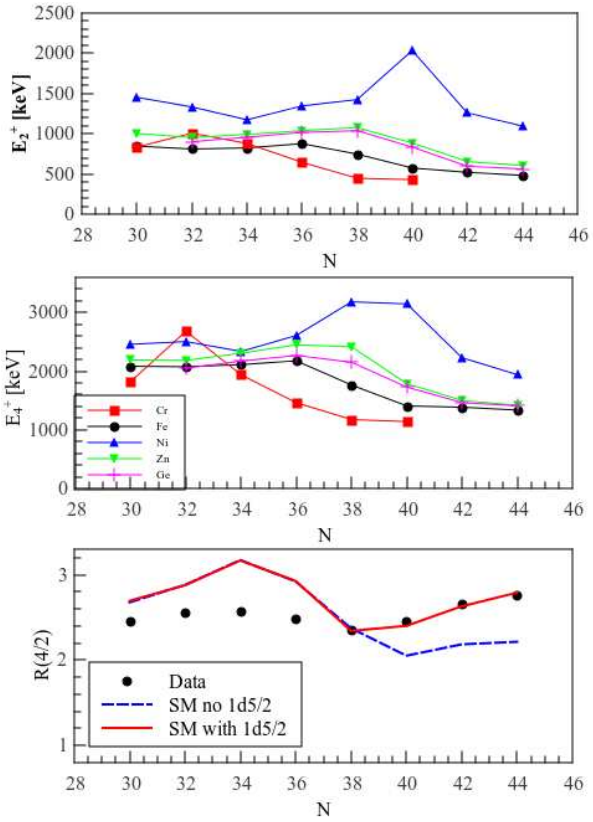


Figure 4: Evolution of the $2^+$ (top panel) and $4^+$ (middle panel) energies in the even Z isotopic chains ranging from Z=24 (Cr) to Z=32 (Ge) (same symbols in the two panels). The bottom panel shows the trend of the ratio $R_{4/2}=E(4^+)/E(2^+)$ in the Fe isotopic chain from N=30 to N=44: black dots correspond to experimental values, while the red (blue) lines show shell-model (SM) predictions including (excluding) the $1d_{5/2}$ neutron orbital in the model space. See text for details.

quadrupole collectivity can be related to the occupation of neutron intruder orbitals which are quasi-SU(3) partners, which are, in this case, the $0g_{9/2}$ and $1d_{5/2}$ orbitals. This is at variance with calculations in Ref. [17] which predict the maximum deformation for mass 68, and is instead well reproduced by the calculations shown in this letter.

The experimental ratios (black dots) are compared with calculations using a 4-orbital neutron model space (dashed blue line) and 5 orbitals (solid red line): the role of the $1d_{5/2}$ neutron orbital is highlighted here, since it is required to get a good placement of the $4^+$ level and, therefore, to reproduce the $R_{4/2}$ ratio. There is a slight deviation of the $4^+$ energies for isotopes below N=38,

which reflects in the deviation of the $R_{4/2}$ for these masses, as shown in the bottom panel of Fig. 4. The fact that the two predictions (including and not including the $1d_{5/2}$ orbital) deviate of the same amount from the experimental $R_{4/2}$ ratio below N=38, imply a non-essential role of this orbital in the description of lighter isotopes in the Fe isotopic chain. It is the inclusion of the neutron $1d_{5/2}$ orbital which favors quadrupole correlations and the development of quadrupole collectivity in the mass region above N=38, and not seen for lighter nuclei.

In conclusion this letter reports on new experimental information on neutron-rich Fe isotopes up to mass 70. Half-lives and $P_n$ values are reported for the first time in mass 70. The $P_n$ values, in particular, show that this decay branch starts to be sizable already in $^{68}$Mn, becoming immediately very large in the heavier systems. Gamma-ray energies for the decay of $^{69}$Fe and $^{70}$Fe are shown for the first time. For the odd isotope the limited statistics do not allow to extract $\gamma - \gamma$ coincidences. Its decay spectrum shows a substantial contribution from the $\beta$-delayed neutron channel, which seems to populate specific low-J states preferentially. By systematics, and supported by recent shell-model calculations, we assign the $\gamma$ rays seen in the spectrum of $^{70}$Fe to the depopulation of the $2_1^+$ and $4_1^+$ levels.

The continuously growing $R_{4/2}$ ratio between the energies of these two levels indicates an increasing collectivity in the Fe isotopic chain, well beyond N=40.

It is found that the experimental $R_{4/2}$ ratio is properly reproduced for A>36 by the shell model only with the inclusion of the $1d_{5/2}$ neutron orbital in the valence space. This is interpreted, as for Cr isotopes, in terms of the interplay between the quadrupole correlations of the $\nu 1d_{5/2}$ and $\nu 0g_{9/2}$ orbitals and the monopole component of the $\pi 0f_{7/2}$ - $\nu 0f_{5/2}$ interaction, thus driving the deformation in the neutron-rich Cr-Fe region.

Since the maximum of quadrupole deformation has not been reached yet, investigating heavier Fe isotopes is of foremost interest to assess the robustness of the N=50 shell closure below $^{78}$Ni.

The excellent work of RIKEN accelerator staff, for providing a stable -very intense- $^{238}$U beam is acknowledged. The project is co-financed by the European Union and the European Social Fund. This work was supported by NuPNET-ERA-NET within the NuPNET GANAS project, under grant agreement No.202914 and from the European Union, within the 7th Framework Program FP7/2007-2013, under grant agreement No. 262010 ENSAR-INDESYS. This work was also supported by Programmi di Ricerca Scientifica di Rilevante Interesse Nazionale (PRIN) number 2001024324_01302. We here acknowledge support from the Spanish Ministerio de Ciencia e Innovacion under Contracts No. FPA2009-13377-C02 and No. FPA2011-29854-C04, the Hungarian Research Fund OTKA contract numbers K100835 and NN104543, the European Commission through the Marie Curie Actions Contract No. PIEFGA-2001-30096 and by Japanese JSPS KAKENHI Grants No. 24740188 and No. 25247045.

## References

[1] T. Otsuka, et al., Phys.Rev.Lett. 95 (2005) 232502.
[2] H. Grawe, et al., Springer Lect. Notes in Phys. 651 (2004).
[3] F. K. Thielemann, et al., Phys. Rep. 227 (1993) 267.
[4] B. Pfeiffer, et al., Nucl. Phys. A 693 (2001) 282.
[5] K. L. Kratz, et al., Ap. J. 403 (1993) 216.
[6] R. Broda, et al., Phys. Rev. Lett. 74 (1995) 868.
[7] O. Sorlin, et al., Phys. Rev. Lett. 88 (2002) 092501.
[8] K. H. Langanke, et al., Phys. Rev. C 67 (2003) 044314.
[9] C. Guènaut, et al., Phys. Rev. C 75 (2007) 044303.
[10] M. Hannawald, et al., Phys. Rev. Lett. 82 (1999) 1391.
[11] P. Adrich, et al., Phys. Rev. C 77 (2008) 054306.
[12] S. N. Liddick, et al., Phys. Rev. C 87 (2013) 014325.
[13] J. Ljungvall, et al., Phys. Rev. C 81 (2010) 061301(R).
[14] W. Rother, et al., Phys. Rev. Lett. 106 (2011) 022502.
[15] O. Sorlin, et al., Eur. Phys. Journal A 16 (2003) 55.
[16] A. Gade, et al., Phys. Rev. C 81 (2010) 051304(R).
[17] S. M. Lenzi, et al., Phys. Rev. C 82 (2010) 054301.
[18] M. P. Carpenter, et al., Phys. Rev. C 87 (2013) 041305(R).
[19] H. L. Crawford, et al., Phys. Rev. Lett. 110 (2013) 242701.
[20] E. Caurier, et al., Eur. Phys. J. A 15 (2002) 145.
[21] L. Coraggio, A. Covello, A. Gargano, N. Itaco, Phys. Rev. C 89 (2014) 024319.
[22] ENSDF, http://www.nndc.bnl.gov (2015).
[23] P. Möller, B.Pfeifer, K.-L. Kratz, Phys. Rev.C 67 (2003) 055802.
[24] H. Koura, T. Tachibana, M. Uno, M. Yamada, Prog. Theor. Phys. 113 (2005) 305.
[25] T. Tachibana, M. Yamada, Proc. Inc. Conf. on exotic nuclei and atomic masses, Arles, France, 1995 (1995) 763.
[26] K. Miernik, Phys. Rev. C 90 (2014) 0543060.
[27] K. Kubo, et al., Nucl. Instr. Meth. B204 (2003) 97.
[28] S. Nishimura, Prog. Theor. Exp. Phys 2012 (2012) 03C006.
[29] P. A. Söderström, et al., Nucl. Instr. Meth. B317 (2013) 649.
[30] Z. Patel, et al., RIKEN Accel. Porg. Rep. 47 (2014) 13.
[31] H. Bateman, Proc. Cambridge Philos. Soc. 15 (1910) 423.
[32] Z. Y. Xu, et al., Phys. Rev. Lett. 113 (2014) 032505.
[33] G. Lorusso, et al., Phys. Rev. Lett. 114 (2015) 192501.
[34] K. Miernik, Phys. Rev. C 88 (2013) 041301(R).
[35] N. Goriely, S Chamel, J. M. Pearson, Phys. Rev. C 82 (2010) 035804.
[36] M. Birch, et al., Nucl. Data Sheet 128 (2014) 131.
[37] J. M. Daugas, et al., Phys. Rev. C 83 (2011) 054312.
[38] B. Olaizola, et al., Phys. Rev. C 88 (2013) 044306.
[39] D. Radulov, Ph.D. thesis, KU Leuven,Faculty of Science, Heverlee (Belgium), 2014.
[40] G. Audi, et al., Nucl. Phys. A 729 (2003) 337.
[41] L. Coraggio, et al., Prog. Part. Nucl. Phys. 62 (2009) 135.
[42] S. Bogner, T. T. S. Kuo, L. Coraggio, A. Covello, N. Itaco, Phys. Rev. C 65 (2002) 051301(R).
[43] J. C. Hardy, et al., Phys. Lett. B 71 (1977) 307.